Marine Geology 369 (2015) 1–18

Contents lists available at ScienceDirect

Marine Geology

journal homepage: www.elsevier.com/locate/margeo

Deep-sea sedimentation offshore eastern Taiwan: Facies and processes characterization

Rémi Lehu [a,b,*], Serge Lallemand [a,c], Shu-Kun Hsu [b,c], Nathalie Babonneau [d,c], Gueorgui Ratzov [e], Andrew T. Lin [b,c], Laurent Dezileau [a,c]

[a] Université de Montpellier, Géosciences Montpellier, 34090 Montpellier, France
[b] Department of Earth Sciences, National Central University, Zhongli, Taiwan
[c] LIA, ADEPT, France–Taiwan
[d] Université de Brest, UMR 6538 Domaines Océaniques, 29280 Plouzané, France
[e] GéoAzur, Université de Nice/Sophia-Antipolis, CNRS, Observatoire de la Côte d'Azur, 06560 Valbonne, France

ARTICLE INFO

Article history:
Received 19 May 2014
Received in revised form 20 May 2015
Accepted 25 May 2015
Available online 26 June 2015

Keywords:
Active margin
Morphosedimentary mapping
Slope instabilities
Turbidites

ABSTRACT

Recent sedimentary facies and processes along the offshore slope of east Taiwan are investigated using a large set of geophysical and sedimentological data. The Taiwan orogen is often considered as one of the most tectonically active regions in the world and also suffers important climatic activity with an average of four typhoons per year. We have mapped in details the morphosedimentary features and characterized the sedimentary facies along offshore eastern Taiwan. There, we show that the slope is driven by a variety of erosional processes from mass wasting to turbidity current. Mass movements such as slides or mass transport deposits (MTDs) are ubiquitous and affect the whole east coast off Taiwan. Detailed core investigations, such as grain size analysis, chemical and mineralogical composition, revealed that turbidite facies range from thin fine-grained turbidites to thick massive turbidite facies. The detailed analysis of turbidite beds allow us to discuss the controlling factors of turbidity current generation. Turbidity currents represent an important sedimentary process that governs the slope morphology off east Taiwan. Triggering mechanisms likely range from slope instabilities related to earthquakes shaking to failure relative to climatic-controlled pulses of sediment supply. We propose that at least two end-members are characteristics in our turbidite records in term of controlling factor:

1) Turbidity currents likely generated by tectonic activity and earthquakes shaking in particular; and
2) Turbidity currents likely generated by climatic activity such as typhoon-induced floods.

1. Introduction

Along active margins, gravity flows represent the main erosional process that controls slope morphology and governs sediment dispersal in the oceanic realm (Masson et al., 2006). Gravity flows include massive debris avalanches (Collot et al., 2001), slide/slumps, cohesive debris flows, fluidized flows (Mulder and Cochonat, 1996; Mulder and Alexander, 2001) and turbulent flows such as turbidity currents (Bouma, 1962; Mulder and Alexander, 2001). These sedimentary processes result in a variety of deposits (slumps, MTDs, Turbidites) and are triggered or facilitated by a wide range of factors including tectonic forcing (uplift and slope oversteepening, earthquakes) and climatic forcing (catastrophic floods, sea-level variations, wave loading, storms, sediment overloading), or a combined effect of both (Einsele, 1996; Locat and Lee, 2002; Piper and Normark, 2009). Additionally, longshore currents may also locally rework, transport and accumulate shelf material or the one supplied by rivers (Romans et al., 2009; Covault and Graham, 2010). The Taiwan mountain belt, represents a peculiar place to investigate such sedimentary processes because it displays a variety of morphological settings, an intense tectonic and seismic activity, and high sedimentation rates (Huh et al., 2004, 2006). Since the last decades, the Taiwan area has been studied through abundant tectonic and geophysical investigations but it appears that only few studies focused on morphosedimentary processes (Huang et al., 1992; Dadson et al., 2005; Ramsey et al., 2006). Because of a lack of "ground-truth" data it is still uncertain to provide a clear assessment about the erosional processes that shape the seafloor offshore eastern Taiwan and their controlling factors. Using a compilation of a large pre-existing geophysical dataset and newly acquired sedimentological data, we aim to characterize the variability of sedimentary facies in such an active context. This work will provide new considerations on

* Corresponding author at: Géosciences Montpellier, Montpellier, France.
E-mail address: lehu.remi@gmail.com (R. Lehu).

http://dx.doi.org/10.1016/j.margeo.2015.05.013
0025-3227/

recent sedimentation and constrain the sedimentary processes. The results will give insights to the controlling factors of such sedimentary processes offshore eastern Taiwan. This work is important for future studies and geohazard assessment such as submarine landslides or hyperpycnal flows that may trigger tsunamis or telecommunication cables breakage (Hsu et al., 2008; Carter et al., 2012).

2. Regional settings

2.1. Geological context

The Taiwan mountain belt results from the rapid and oblique convergence of the Luzon arc carried by the Philippine Sea Plate (PSP), and the passive Chinese continental margin (CCM, Fig. 1A) (Biq, 1972; Suppe, 1984). Plate kinematics predicts about 80 mm/year of convergence between these two plates (Seno et al., 1993). The orogen links two subduction systems dipping with opposite vergence: to the South the Manila subduction zone and to the east the Ryukyu subduction zone (Fig. 1A). South of Taiwan, the South China Sea lithosphere is being subducted eastwards beneath the PSP, building an accretionary wedge progressively uplifted above the sea level. To the northeast, the PSP slab is retreating southwards beneath the Eurasian margin resulting on the opening of the Okinawa back-arc domain and the collapse of the northern part of the Taiwan mountain belt.

2.2. Regional climate, drainage systems and sediment discharge

Taiwan is positioned within the "Typhoon Alley" (Liu et al., 2008) and is impacted on average by three or four typhoons annually. Therefore, Taiwan receives not only abundant precipitation due to its southern Asian monsoon climate, but periodically heavy rains during typhoons (Wu et al., 1999; Lin et al., 2002; Galewsky et al., 2006; Liu et al., 2008). The Morakot Typhoon (2009) was the worst event of the last 50 years with a 2777 mm accumulated rainfall (Ge et al., 2010). It triggered 12,697 landslides (Tsou et al., 2011; Wu et al., 2011) and exceptional flooding in Southern Taiwan, and left 700 casualties and catastrophic damages. The east flank of the Central Range is drained by rivers, incising the geological units. The Coastal Range, elongating along the east coast of Taiwan, represents a dam and captures the rivers. The runoff collected along the Longitudinal Valley (Fig. 1B) is diverted around the northern and southern edges of the Coastal Range in the Hualien and Beinan rivers respectively. The Hsiukuluan river is the only drainage cutting through the Coastal Range. Northeast of Taiwan, the Hoping and the Liwu rivers (Fig. 1B) are the major rivers collecting the runoff from the Central Range. In Southeastern Taiwan, the Taimali River and smaller rivers (e.g Jinlun river, Nongxi river, Dawu river and Daren river, see Fig. 1B for location) accumulate most of the runoff from the Hengchun Peninsula (Fig. 1B). With high relief, steep gradients, important tectonic activity, heavy rainfall and frequent typhoons, Taiwan has the highest sediment production worldwide, and possesses 7 of the 10 global rivers with the highest sediment yield (Li, 1976; Milliman and Syvitski, 1992; Chen et al., 2004; Dadson et al., 2004; Liu et al., 2008). Taiwanese rivers presently annually discharge >300 Mt of sediments to the surrounding ocean and >30% of the total sediment from Taiwanese rivers is discharged at hyperpycnal concentrations (Dadson et al., 2005; Kao and Milliman, 2008; Liu et al., 2008). The river discharges on the east coast of Taiwan reaches about 150 Mt/year (Liu et al., 2008).

2.3. Submarine morphology

The morphology off eastern Taiwan displays a complex interaction between onshore and offshore processes in a context of high tectonic activity and extreme tropical rainfalls. From latitude 22°N to 24.5°N, the margin includes a flat narrow shelf, a steep incised slope, oceanic basins and sedimentary ridges such as the Huatung ridge and the Hsincheng ridge (Fig. 1B). The shelf is <10 km-wide, with a slope break at ~100 m water-depth. The slope displays steep slope gradients (15 to 20°) and is deeply incised by gullies and canyons (Fig. 1B). Downslope, they merge to form a dendritic channel pattern transferring sediments to deep oceanic basins (Ramsey et al., 2006). The slope also

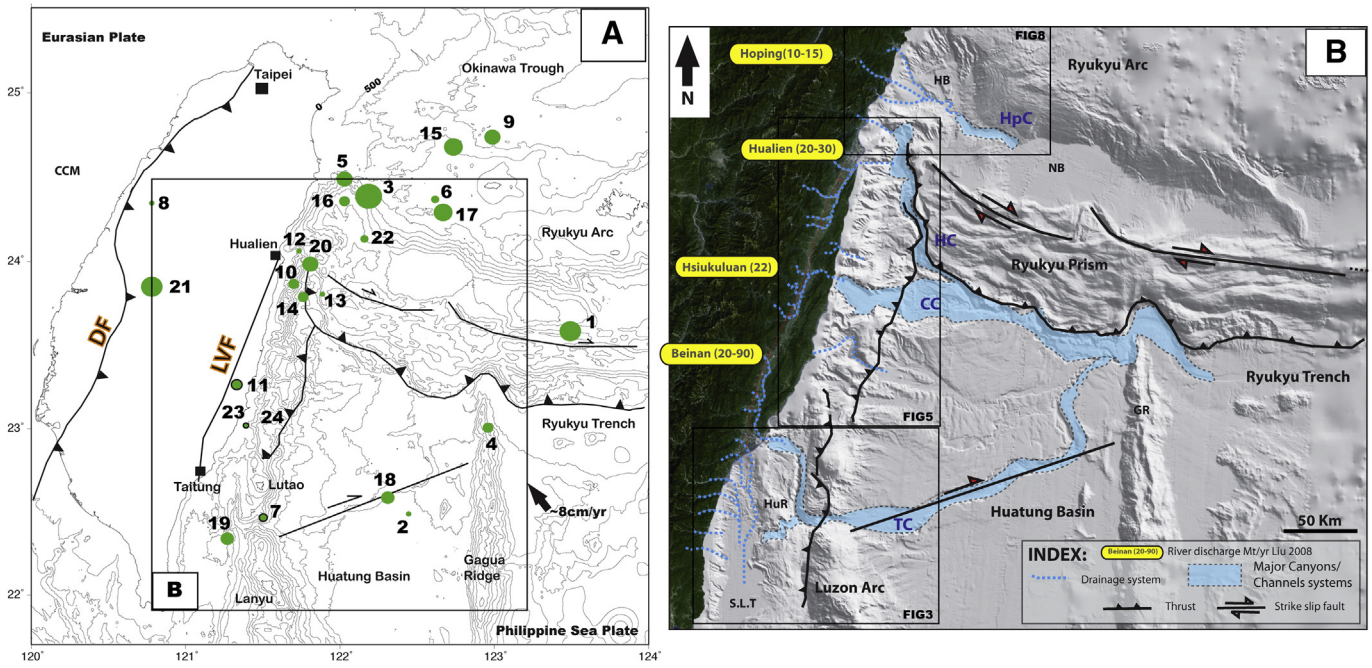

Fig. 1. A: Geodynamic context of Taiwan and plate boundaries, the box represents a zoom on the study area shown in B. CCM = Chinese continental margin, DF = Deformation Front, LVF = Longitudinal Valley Fault. The green circles represent the major earthquakes (Mw > 6.8) that struck the Taiwan island during the 20th century. Bathymetry is represented with contour line every 500 m and derived from the ACT96 survey; B: Recent sedimentary systems offshore eastern Taiwan showing the main active canyons and the actual drainage system. In yellow boxes are represented the river discharge in Mt/year after Liu et al. (2008). HB = Hoping Basin, NB = Nanao Basin, SLT = Southern Longitudinal Trough, HuR= Huatung Ridge, TC= Taitung Canyon, CC= Chimei Canyon, HC= Hualien Canyon, HpC= Hoping Canyon. (For interpretation of the references to color in this figure legend, the reader is referred to the web version of this article.)

exhibits escarpments associated with tectonic structures such as thrusts and folds (Malavieille et al., 2002). The drainage systems involve three major submarine canyons collecting the sedimentary discharge from the Central Range and the Coastal Range; from north to south, the Hualien Canyon, the Chimei Canyon and the Taitung Canyon (Fig. 1B). Additionally, numerous channels incise the continental slope and merge with the canyons. They do not seem to be connected with subaerial drainage systems. Their morphological characteristics, extensively described by Ramsey et al. (2006), suggest that marine erosional processes such as submarine landslides, debris flows or turbidity currents might be dominant.

2.4. Seismic activity

The seismicity rate is extremely high: during the last century, 22 Mw > 7 earthquakes occurred onshore and offshore (Fig. 1A, Table 1) (Cheng and Yeh, 1989; Engdahl and Villaseñor, 2002; Theunissen et al., 2010). Offshore, the greatest event ever recorded in the Ryukyu margin was estimated with a magnitude Mw 7.7 (Theunissen et al., 2010). Such seismic activity has necessarily direct influences on shaping the offshore morphology and consequently on the driving mechanisms of the present offshore sedimentation. Moreover, earthquakes may not only directly trigger gravity flows but they should also represent a favoring factor that contributes to the supply of material and the loading of the slope.

2.5. Oceanic setting

The oceanography in Taiwan is dominated by the Kuroshio Current, which extends from the northern Philippines to the Japanese archipelago, passing the east coast of Taiwan. East of Taiwan the current may reach a depth of 1000 m at some latitudes and the mean Kuroshio transports are 30 ± 5 Sv (1 Sv = 106 $m^3.s^{-1}$) with annual mean surface rates, between 0 and 50 m, reaching up to 1.3 $m.s^{-1}$ (~2.5 knots) at a distance between 20 and 40 km from the east coast of Taiwan (Hsin et al., 2008). The main branch then turns east after passing along Taiwan to follow the Okinawa Trough. This important oceanic current will thus play a role in the transport of suspended material along the offshore east Taiwan.

Table 1
Mw ≥ 6.8 earthquakes recorded over the instrumental period (20th century) in the studied area. References for the location origin: 1. (Engdahl and Villaseñor, 2002); 2; (Theunissen et al., 2010); 3. (Cheng and Yeh, 1989); 4. (Cheng et al., 1996; Chen and Tsai, 2008); 5.(Wu et al., 2008). (*) M'w: equivalent moment magnitude determined by Theunissen et al. (2010).

Eq. number	Date (yy/mm/dd)	Lon. (°)	Lat. (°)	Depth (km)	M'w (*)	Source
1	1915/2/28	123.50	23.60	0	7.5	1
2	1919/12/20	122.50	22.50	35	6.9	1
3	1920/6/5	122.22	24.29	35	7.7	2
4	1921/4/2	123.00	23.00	35	7.1	1
5	1922/9/1	122.04	24.50	35	7.3	1
6	1922/9/14	122.64	24.370	35	7	1
7	1935/9/4	121.55	22.50	20	7	3
8	1935/4/20	120.82	24.35	5	6.9	3
9	1947/9/26	123.00	24.75	110	7.3	1
10	1951/10/21	121.72	23.87	4	7.1	4
11	1951/11/24	121.35	23.27	36	7.1	4
12	1951/10/22	121.72	24.07	1	6.9	4
13	1951/10/22	121.95	23.82	18	6.9	4
14	1957/2/23	121.80	23.80	30	7.1	3
15	1959/4/26	122.79	24.68	126	7.5	1
16	1963/2/13	122.06	24.35	35	7.1	1
17	1966/3/12	122.69	24.30	28	7.5	1
18	1972/1/25	122.32	22.54	10	7.3	1
19	1978/7/23	121.32	22.35	6	7.2	3
20	1986/11/14	121.83	23.99	15	7.3	3
21	1999/9/20	120.80	23.85	6	7.6	5
22	2002/3/31	122.16	24.16	16	7	5
23	2003/12/10	121.38	23.07	21	6.8	5

3. Materials and methods

3.1. Bathymetry, backscatter and seismic data

Multibeam bathymetry and side-scan backscatter imagery were obtained during the ACT (Active Collision Taiwan) survey in 1996 onboard of the *R/V L'Atalante* (Lallemand and Tsien, 1997) (Fig. 2) using a SIMRAD EM12-Dual and EM950 (for depths shallower than 300 m) multibeam systems that enable swath mapping and backscatter imagery. Chirp seismic reflection data have been recorded during the OR1-1013 survey in September 2012 allowing us to characterize the seismic facies of the first meters below the seafloor. Moreover a set of multichannel seismic reflection lines acquired during several cruises between 1993 and 2012 is used in this study (Table 2, Fig. 2).

3.2. Cores

Ten gravity and piston cores were collected off eastern Taiwan during the OR1-1013 and the OR1-1048 surveys (Fig. 2). Deposits were described with a particular attention to grain size distribution variation and turbidite/hemipelagite differentiation. Grain size analyses were performed every 2 to 0.5 cm using a Coulter LS13 320 laser microgranulometer (size range from 0.4 μm to 2 mm). To accurately identify the sedimentary structures and the chemical composition, X-Ray radiography and XRF measurements were performed using an ITRAX Core Scanner at 2 mm interval. The composition of the sand fraction (>63 μm) of turbidites was analyzed using a stereomicroscope on wet sieved 1 cm-thick samples collected at the base of selected turbidites. Additionally, to enhance the core coverage we used published data from the area (Fig. 2): 7 box-cores collected onboard R/V Ocean Researcher I (1989) (Huang et al., 1992); 5 cores collected during the OR1-960 survey and 1 box-core from OR1-687 (Huh et al., 2004).

4. Description of sedimentary features revealed by geophysical data

Detailed mapping based on bathymetry, backscatter imagery and seismic data shows three sectors with distinct sedimentary features: the southern, central and northern sectors (Fig. 2). This mapping highlights the distribution of sedimentary structures indicating erosional and depositional processes.

4.1. The southern sector

4.1.1. Submarine canyons

The Taitung canyon is the major canyon offshore eastern Taiwan. It incises the upper slope, crosses the Luzon Arc and the Huatung Basin to end in the Ryukyu Trench (Fig. 1B). The Taitung canyon contains three parts S1, S2 and S3 (Fig. 3B):

- S1 is the head of the canyon (Fig. 4). Four km wide, it exhibits a high reflectivity (Fig. 3A). It runs from 500 m water depth down to 1500 m and is directly fed by the major Beinan River onland and a small river from the Coastal Range (Fig. 1B, River 9 on Fig. 3B and River 10 Fig. 5B).
- S2 runs from 1500 m water depth down to 3000 m. It has a rough, sinuous and narrow (2 km wide) bed with a V-shape incision and is characterized by a highly reflective seafloor (Figs. 3A, 4B). Well-developed levees are observable on both sides of S2 (Fig. 4B). It is fed by tributary meandering canyon (C1) incising the Huatung sedimentary ridge (Fig. 3B) (Malavieille et al., 2002). The canyon C1 also exhibits a high reflectivity (Fig. 3A).
- S3 presents a different pathway with a W–E orientation, cutting through the Luzon Arc between the volcanic islands of Lutao and

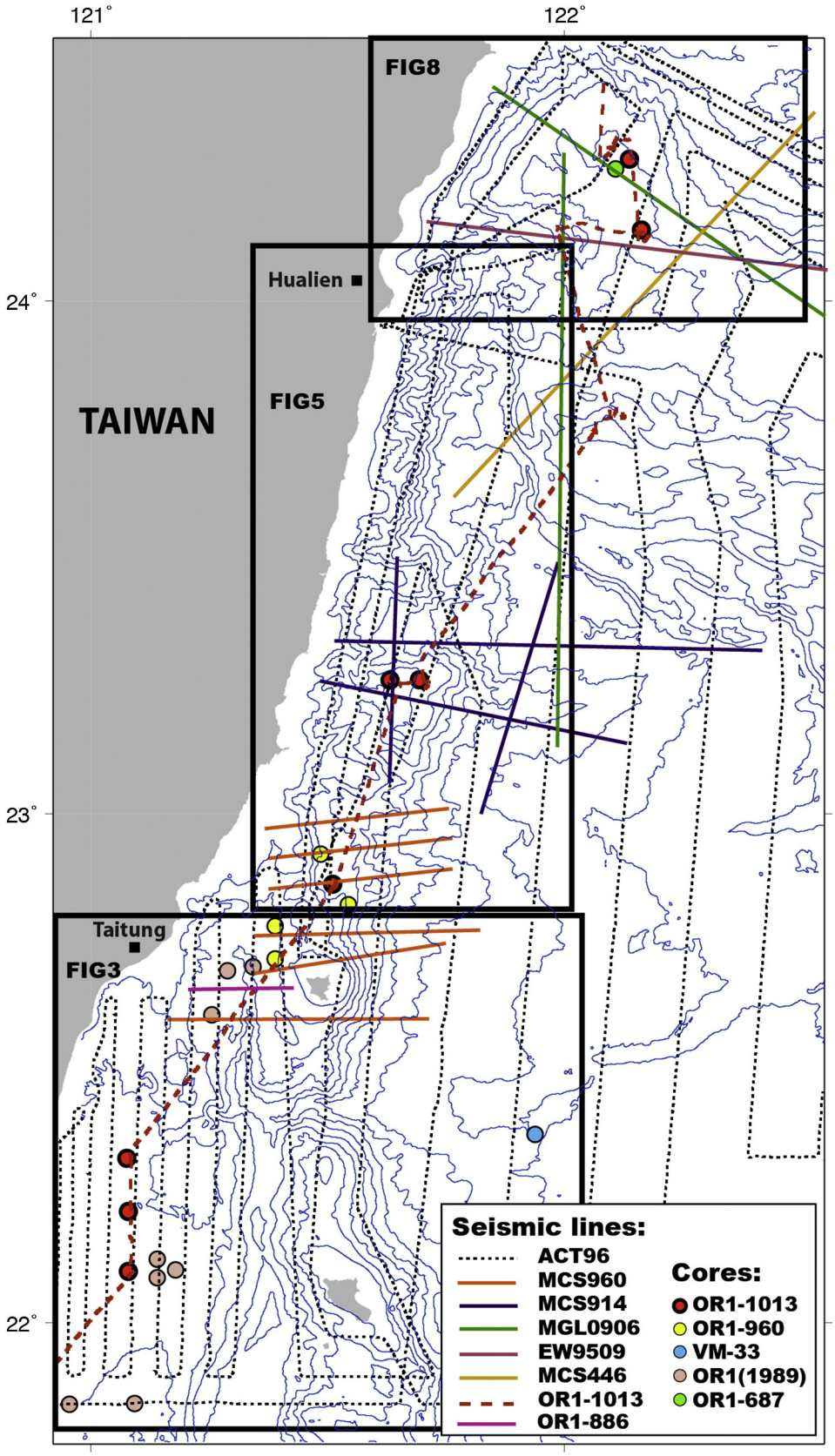

Fig. 2. Location of seismic, CHIRP profiles and sedimentary cores. The bathymetry is represented with contour lines every 500 m and derived from the ACT96 survey.

Lanyu and extending to the Huatung Basin (Figs. 1, 3). When crossing the Luzon Arc, the canyon shows a narrow (4 km wide) V-shape incision, up to 1500 m-deep. In the Huatung Basin, the upper part of S3 is fan shaped and its channel width decreases from 14 km down to 7 km downstream (Schnurle et al., 1998). The floor of the canyon appears to be very rough as shown by the high to moderate

Table 2
List of available seismic lines in the study area.

Vessel	Year	Survey	References
Ocean Researcher I	1993	OR1-376	(Lallemand et al., 1997)
Ocean Researcher I	1996	OR1-446	(Font et al., 2001; Font and Lallemand, 2009)
L'Atalante	1996	ACT96	(Lallemand et al., 1999; Malavieille et al., 2002; Ramsey et al., 2006)
Maurice Ewing	1995	EW-9509	(Mcintosh and Nakamura, 1998; Schnürle et al., 1998; Wang and Chiang, 1998; Font et al., 2001; Hetland and Wu, 2001; Wang et al., 2004; McIntosh et al., 2005; Font and Lallemand, 2009)
Ocean Researcher I	2009	OR1-886	*This study*
Ocean Researcher I	2009	OR1-914	*Unpublished*
Ocean Researcher I	2010	OR1-960	*This study*
Marcus Langseth	2009	MGL-0905	(Lallemand et al., 2013)
Ocean Researcher I	2012	OR1-1013	*This study*

This study means the seismic lines we presented in the paper. *Unpublished* are the seismic lines used in this work that have not been published.

reflectivity (Fig. 3A). In the Huatung Basin, a channel-levees system parallels the main (Fig. 3B).

4.1.2. Turbiditic system

The Southern Longitudinal Trough (hereafter called SLT) is a proximal orogenic basin developed in a forearc position (Malavieille et al., 2002). This basin is a N–S elongated basin (Figs. 1, 3) 90 km long and 15 km wide. The SLT is bounded to the west by the slope of the Hengchun peninsula and to the east by the Huatung sedimentary ridge (HuR on Fig. 1B). A narrow shelf fringes the SLT with an abrupt shelf break at 100 m of water depth (Fig. 1B). A network of straight E–W trending gullies feed two straight to meandering N–S trending channels. Gullies form a badland topography and show a high reflectivity (Fig. 3A). They are observed at different scales from tens of meters to

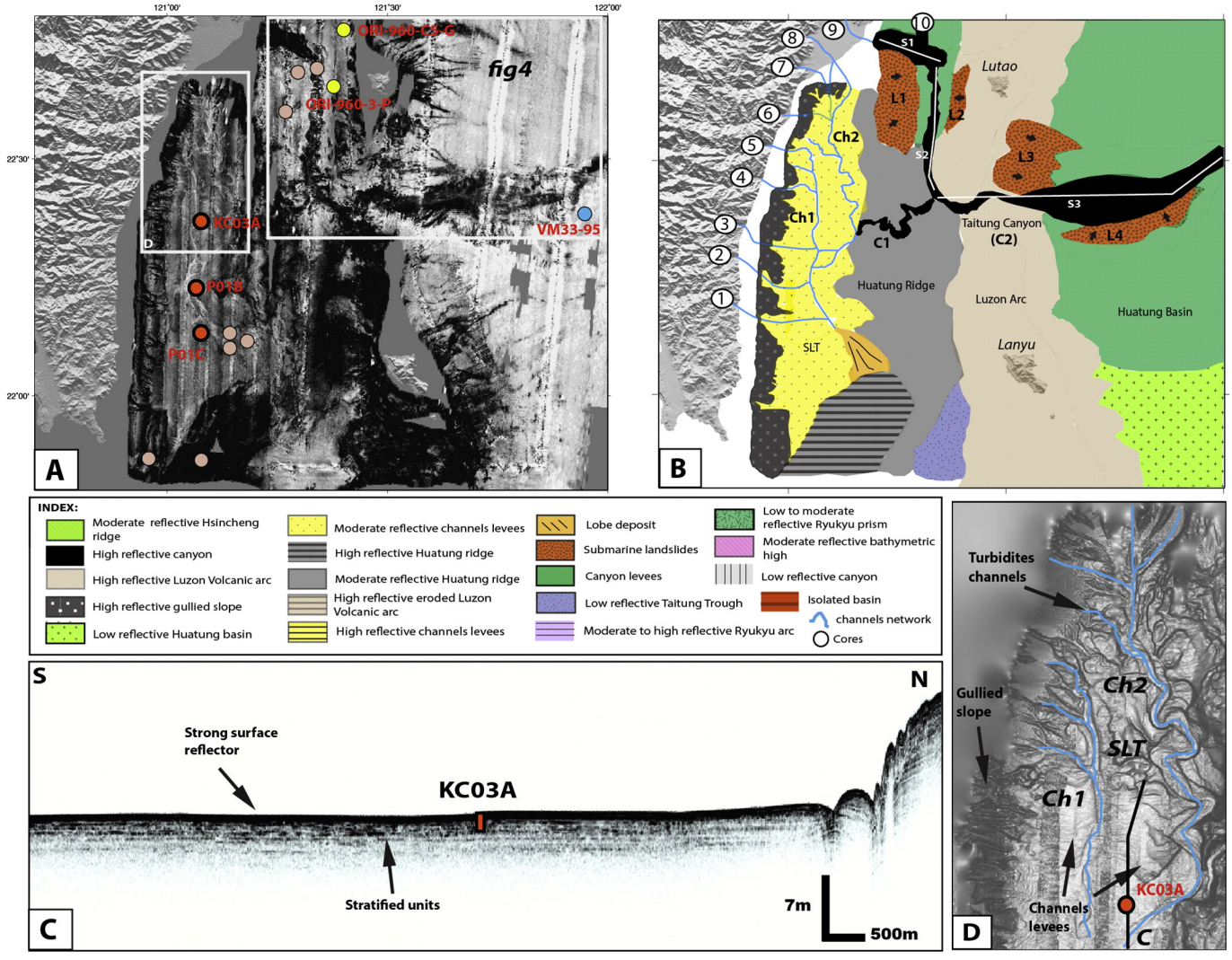

Fig. 3. A: Backscatter imagery of the southern sector. On backscatter images, dark tones indicate high backscatter. The circles represent the sedimentary cores. Boxes indicate zoom on high resolution DEM and features presented in this work; B: Morphosedimentary mapping based on backscatter imagery, seismic and CHIRP data and high resolution DEM. The annotated circles represent the east coast rivers: 1. Xuhai river, 2. Daren river, 3. Dawu river, 4. Nangxi river, 5. Jinlun river, 6. Taimali river, 7. Zhiben river, 8. Taiping river, 9. Beinan river, 10. Donghe river. Ch = Channel, L = Landslide; C = Canyon, S = Canyon section, SLT= Southern Longitudinal Trough. Black arrows represent the inferred landslides movements; C: CHIRP profile across the Southern Longitudinal Trough, showing acoustic facies of sedimentary levee. Track of the profile is located on D; D: high resolution DEM across the Southern Longitudinal Trough showing the well-developed channel-levee system. See Fig. 2 for the location of this zone.

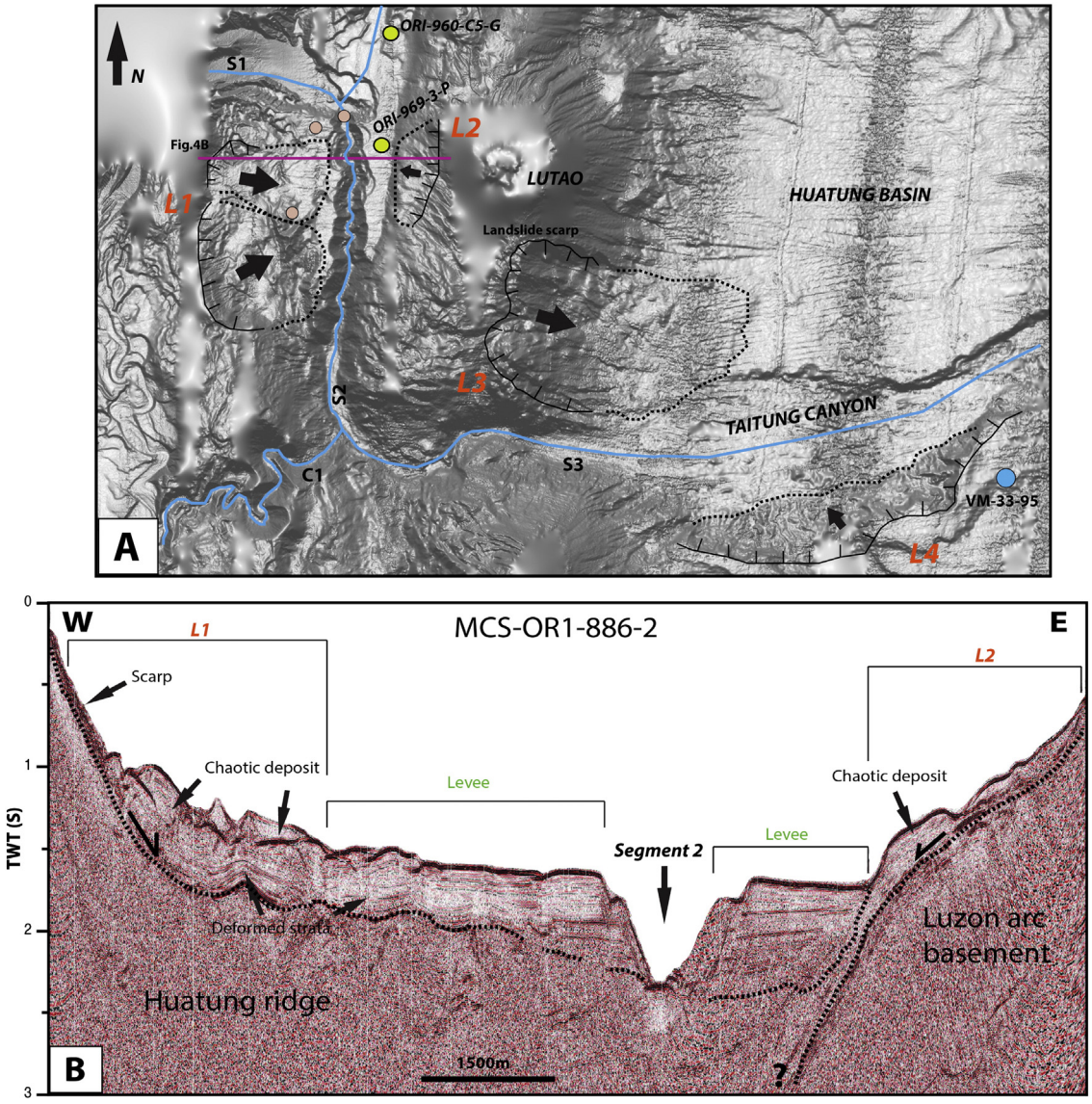

Fig. 4. A: Zoom on high resolution DEM showing submarine landslides affecting the Taitung Canyon (L4), the slope of the Luzon Arc (L3, L2) and the Huatung Ridge (L1). Black arrows represent the inferred landslides movements. Circles represent sedimentary cores in the area; B: Seismic reflection profile across the Taitung Canyon (S2), showing the slope affected landslide on the Luzon Arc and the Huatung ridge. The levees of the Taitung Canyon are also well observable. See Fig. 3 for location.

several hundreds meters. We identify channel-levees complexes on the SLT seafloor. Narrow channels from the western and northern slopes fed by the Taimali and smaller rivers from the Hengchun peninsula (Figs. 1b, 3B). They form a complex channel-levees systems (Fig. 3C, D). Two main channels (Ch1 and Ch2 on Fig. 3D) are parallel to the western slope of the SLT. The channel Ch1 is 20 km long with a low reflectivity (Fig. 3A). It is mainly fed by the Jinlun (River 5 on Fig. 3B). Other tributary channels fed by smaller onland rivers (e.g. River 1, 2, 3, and 4 on Fig. 3B) merge to the main channel Ch1 (Fig. 3B). Channel Ch2 is 30 km long and sinuous in its upper part. It becomes linear downslope (Fig. 3A, D) and is mainly fed from north to south by the Taiping, the Zhiben and Taimali rivers (Rivers 8, 7 and 6 respectively, Fig. 3B). It is characterized by a low reflectivity (Fig. 3A). Downslope, both channels merge and end 15 km afterward, into a sedimentary lobe identified by a low to moderate reflectivity (Fig. 3A). Well-developed sedimentary levees (<100 m-high) are observed along the channels, characterized by moderate reflectivity (Fig. 3A). On echosounder profiles, levees correspond to continuous and high amplitude seabottom reflectors evolving into a stratified echo-facies in depth (Fig. 3C).

4.1.3. Mass-movements deposits

The slope is affected by mass movements, including slide/slumps and mass transport deposits (MTDs hereafter). Mass movements in the form of slumps or MTDs are observable in shallow sediment on (i) the northernmost part of the Huatung ridge (L1 on Figs. 3B, 4A, and b), (ii) the slope of the Luzon Arc (L3 and L2, on Figs. 3B, 4A) and (iii) the southern wall of the segment 3 of the Taitung canyon (L4 on Figs. 3B, 4A). (i) The northernmost edge of the Huatung ridge exhibits a submarine landslide as shown by the seismic profile on Fig. 4B. The slide L1 is characterized by a steep scarp marked by an arcuate shape, and chaotic reflectors packages interpreted as slumped materials (Fig. 4B). (ii) 25 km-wide arcuate scars displaying a steep slope (20–30°) affect the western and the eastern slope (Slide L2 and L3) of the Luzon Arc (Fig. 4A, B). The chaotic reflector packages at the base of the scars supports slope failures (Fig. 4A). (iii) Slides on canyons flanks are common (Mountjoy et al., 2009). The southern flank of the Taitung canyon in the segment 3 shows a 30 km-large scar and a gullied slope (L4) supporting a collapse of the canyon levee (Fig. 4A).

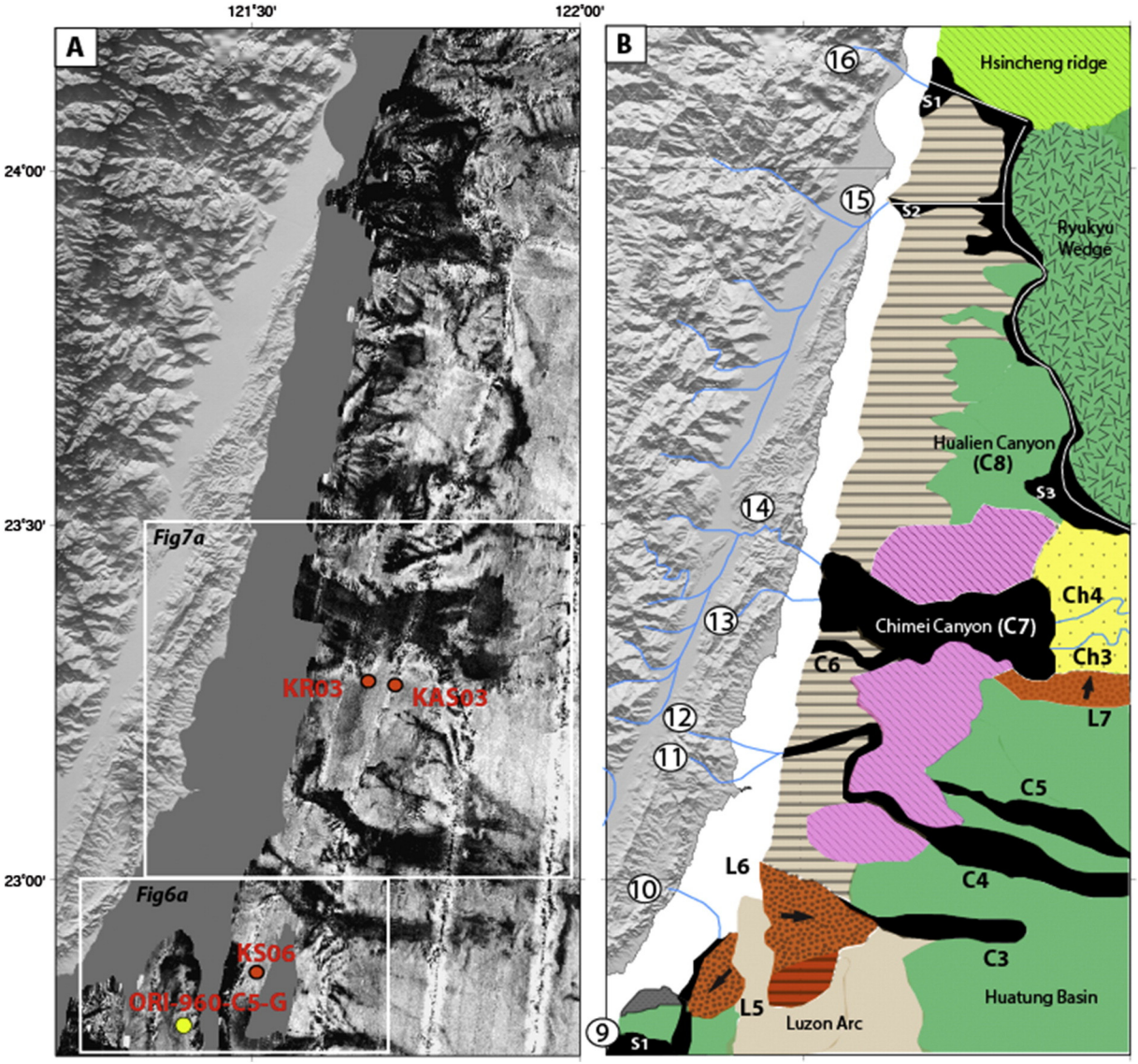

Fig. 5. A: Backscatter imagery of the central sector. On backscatter images, dark tones indicate high backscatter. Circles represent sedimentary cores in the area; B: Mapping of the central sector, using backscatter imagery, seismic data and bathymetry data. Annotated circles represent all the rivers identified in that sector. 9. Beinan river, 10. Donghe river, 11. Sanxiantan river, 12. Wushibi river, 13. Baxiandong river, 14. Xiukuluan river, 15. Hualien river, 16. Liwu river. Black arrows represent the inferred landslides movements. Key is the same as Fig. 3. See Fig. 2 for the location of this sector.

4.2. The central sector

The central sector corresponds to the collision zone of the Luzon Arc with the Chinese continental margin (Malavieille et al., 2002). It includes the Coastal Range and its submerged eastern flank, the western edge of the Ryukyu accretionary wedge and the abyssal Huatung Basin (Fig. 1).

4.2.1. Submarine canyons

The Hualien canyon (C8 on Fig. 5B) is N–S oriented and crosses the Ryukyu accretionary wedge to join the Ryukyu Trench (Figs. 1B, 5). This canyon is divided into three segments, S1 to S3:

- S1 corresponds to the major canyon head, fed by the Liwu river (River 16 in Fig. 5B). It is V-shaped, 4–5 km wide and displays a high reflectivity (Fig. 5A).
- S2 corresponds to a tributary canyon merging with S3 (Fig. 5B). It is fed by the Hualien river (River 15, Fig. 5B) and all its tributary rivers draining the northernmost tip of the Longitudinal Valley of Taiwan. S2 is V-shaped, narrow (1–2 km wide) with a high reflectivity (Fig. 5A).
- S3 is N–S oriented and crosses the Ryukyu accretionary wedge. It has a V-shape section and a high reflectivity on backscatter imagery (Fig. 5B). The northern part of S3 is 6 km wide and becomes narrower and sinous in its southern parts (Fig. 5B). Sedimentary levee developed on the western flank of S3 is characterized by a low to moderate reflectivity (Fig. 5A).

The Chimei "Canyon" (C7) (Figs. 1B, 5 and 7A) incises the submarine slope of the Coastal Range. It is a 10 km wide, U-shape valley. It is fed by the only river cutting through the Coastal Range, the Hsiukuluan river and by a smaller local river (Rivers 14 and 13 respectively, Fig. 5B). The canyon C6 (Fig. 5) meets the Chimei valley on its southern flank. It has a V-shape incision and is characterized by high reflectivity. It does not seem connected to any rivers from the Coastal Range.

The Chimei canyon feeds two meandering channel-levees systems: Ch3 connected to C6 and Ch4 connected to C7 (Figs. 5B and 6A).

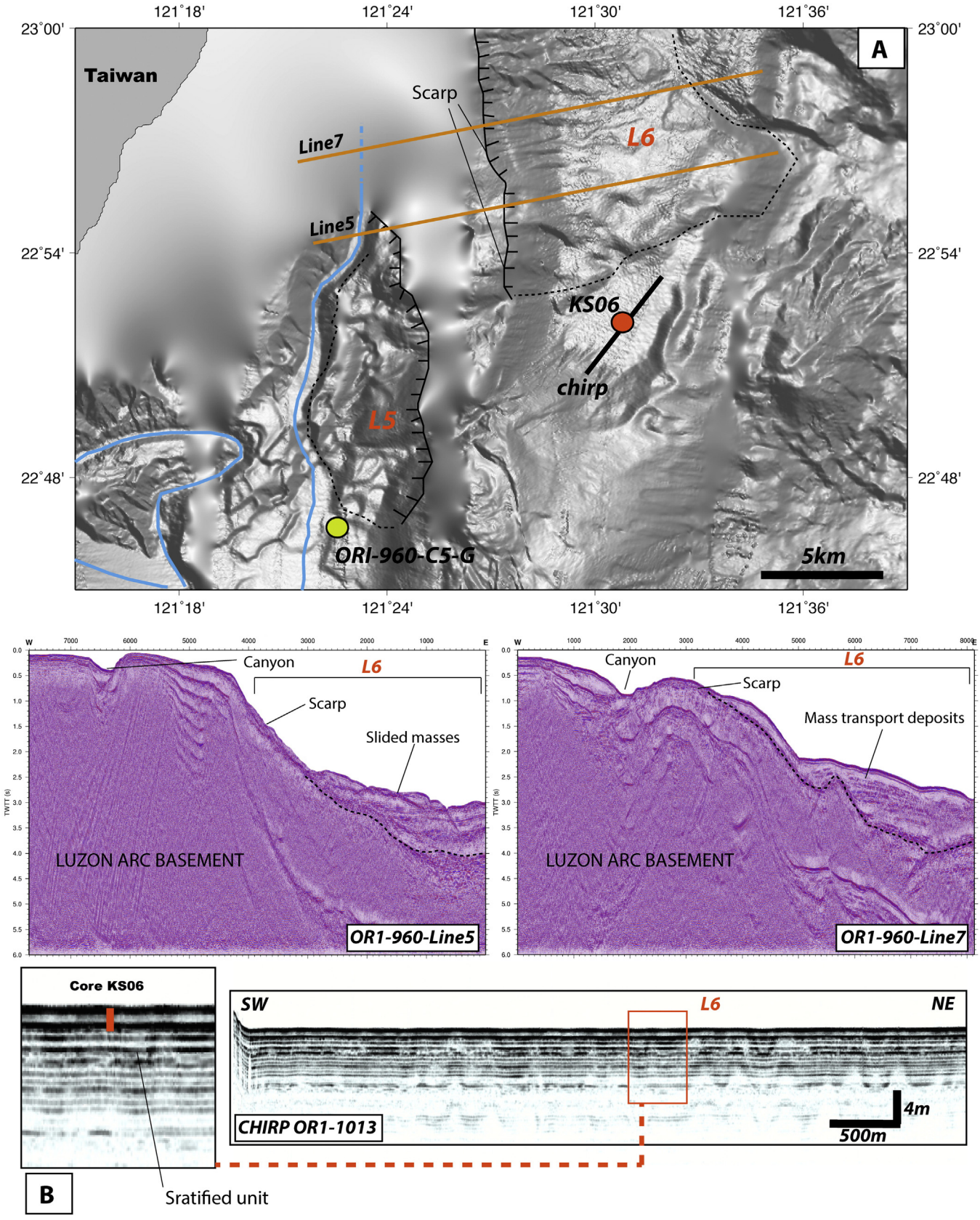

Fig. 6. A: High resolution DEM showing area affected by landslides on the deforming Luzon arc. Circles represent sedimentary cores in the area. Hatched lines show the landslides area; B: Seismic reflection profiles and CHIRP profile displaying seismic facies of landslide and stratified units of the basin-fill sediment respectively. See Fig. 5 for location.

Bathymetric highs with moderate reflectivity are visible on the southern and northern flanks of the Chimei canyon (Figs. 5A and 7A). On chirp profiles, these highs display stratified reflectors (Fig. 7B). Other canyons C3, C4 and C5 also incise the Huatung basin. They are from 2 to 5 km wide, V-shape and show high reflectivity. Levees are visible on the both sides of these canyons with a moderate to low reflectivity (Fig. 5B). Canyon C4 is connected to two small rivers onland from the Coastal Range (Rivers 11 and 12, Fig. 5B). The others are not fed by onland rivers. Erosive features such as submarine valleys incising the offshore lower slope of the Coastal Range (Figs. 6A and 7A) have been extensively described by Ramsey et al. (2006). These features are characterized by high reflectivity on backscatter imagery suggesting intense erosion and steep slopes (Fig. 5A).

4.2.2. Mass-movements deposits

Mass-movements also affect the submarine slope of the Coastal Range (L5, L6 and L7 Figs. 5B, 6 and 7A). Landslides L5 and L6 are characterized by head scarps on seismic lines 5 and 7 (Fig. 6B) as well as transparent and chaotic reflectors packages suggesting slumped or slid masses, or buried mass transport deposits (Fig. 6B). A small perched

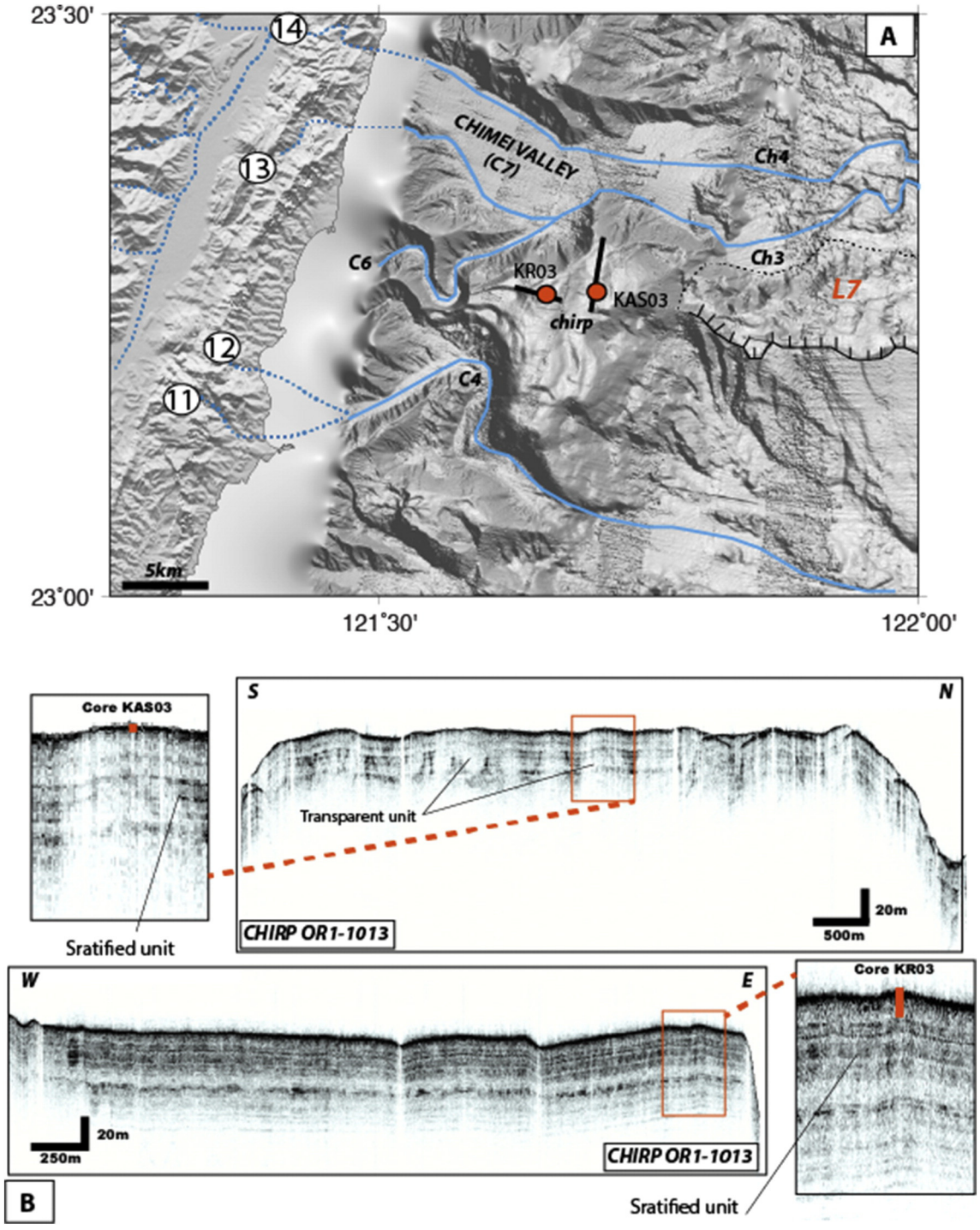

Fig. 7. A: High resolution DEM showing the Chimei turbiditic system with landslide affecting the northern flank of the deep sea fan and bathymetric highs. Circles represent the sedimentary cores in the area; B: CHIRP profiles imaging the bathymetric high. See Fig. 5 for location.

basin is present on the Luzon Arc (Fig. 6A). Chirp profile across the basin show high amplitude reflector at seabottom and well-stratified reflectors in depth. The basin fill sediments (Fig. 6B) are not affected by the large scale slumped deposit observed northward. Downslope the Chimei Valley, a slope failure is also observed southward from the channels-levees system described above (L7 on Figs. 5B and 6A).

4.3. The northern sector

The northern sector includes the western termination of the Ryukyu accretionary wedge, forearc basins and the Ryukyu arc. From west to east, we distinguish the Hoping Basin (HB) and the Nanao Basin (NB) respectively (Figs. 1, 8).

4.3.1. Submarine canyon

The Hoping Canyon (C9) (Figs. 8, 9) crosses the forearc domain ensuring the sediment transit between the two forearc basins (HB and NB). It exhibits a U-shaped morphology and is 3–4 km wide. The Hoping canyon starts from the southeastern edge of the HB, runs almost parallel to the Ryukyu arc and finally reaches the NB that is characterized by a moderate reflectivity. The Hoping canyon is structurally controlled by faults cutting through the entire margin (Font and Lallemand, 2009). By contrast with the other canyons previously described, the Hoping canyon displays a low reflectivity (Fig. 8A). Sedimentary levees are identified on chirp profile on its northern and southern flanks of the canyon (Figs. 8B, 9) and are characterized by moderate reflectivity.

4.3.2. Turbidite channels

The western slope of the HB is strongly eroded and affected by gullies. They ensure the sediment transit from two rivers onland (rivers 17 and 18) to the offshore basins. They are characterized by a very strong reflectivity (Fig. 8A). Downslope, connected to the head of the Hoping canyon, a channel-levees system develops in the HB. Three main channels Ch5, 6 and 7 respectively incise the steep (18–20°) western slope of the HB. Ch5 and Ch6 are connected with major rivers (Rivers 17 and 18 respectively on Fig. 8B) whereas Ch7 seems not being connected to any river. All the channels have built sedimentary levees characterized by moderate reflectivity and by stratified reflectors (Figs. 8B, 9). The HB is bordered on its southern edge by an uplifting sedimentary ridge (Malavieille et al., 2002) characterized by moderate reflectivity, the Hsincheng Ridge (Fig. 8A).

4.3.3. Mass-movements deposits

The slope of the Ryukyu arc is affected by several mass-movements mapped L8, L9 and L10 respectively (Figs. 8B, 9). Arcuate scarp shapes are recognizable above landslides L8, L9 and L10 but not well defined as shown on DEM on Fig. 9. Another landslide (L11) affects the western slope of the Hoping Basin and is characterized by a high reflectivity (Fig. 8A, B).

5. Characterization and classification of lithofacies

In this section, we describe the variability of sedimentary facies along the offshore eastern Taiwan. We intend to address and characterize the lithofacies based on both sedimentological data studies such as visual description, grain size variation, chemical composition and sand fraction content (Figs. 10 and 11), and preexisting cores analysis found in the literature.

5.1. End-members lithofacies

We propose two end-member lithofacies distinguished and qualified as following:

Facies I: hemipelagic sedimentation

Facies I (Fig. 11) is composed of homogeneous clay with low content of silty sediment (<20% of the facies described in cores) and contains diluted foraminifera and sometimes bioturbations. Inconspicuous laminations are present but do not correspond to grain-size changes. Hemipelagites in core are usually characterized by the finest median grain size (<10 μm). This facies is interpreted as the background sedimentation of deep-sea environment.

As a good example, the core KR03 located on a top of a bathymetric high (Figs. 5B, 7) is mainly composed by homogeneous clay and thus dominated by hemipelagic deposits (Fig. 10). In the low reflective Taitung Trough mapped on Fig. 3B, pelagic mud seems to dominate as described by Huang et al. (1992). In the Huatung Basin mapped on Fig. 3B, available data available from core VM 33–95 (Fig. 3A), acoustic and seismic signatures suggest that it is mainly characterized by Facies I.

Facies II: turbidites

Facies II together with Facies I, dominate the sedimentary record. Turbidites are recognized by their coarser grain size and a typical fining upward trend (Fig. 11), defined by the Bouma sequence (Bouma, 1962) and the classification of Stow and Shanmugam (1980). In our cores, turbidite thickness ranges from 1 to about 30 cm (described in Section 5.2). Turbidites are usually interbedded with hemipelagites (Facies I) or stacked. The basal boundaries are easily identified from a change to coarser-grain size and darker color of the sediment. All the cores are characterized by Facies II and found in different sedimentary settings.

5.2. Turbidite facies

According to visual description, grain size analysis, chemical and mineralogical composition, we are able to defined four main turbidites facies:

- *TI*: thin silty-clay lithogenic turbidites;
- *TIIa*: thin silty to fine sand lithogenic turbidites;
- *TIIb*: thin silty to fine sand biogenic turbidites; and

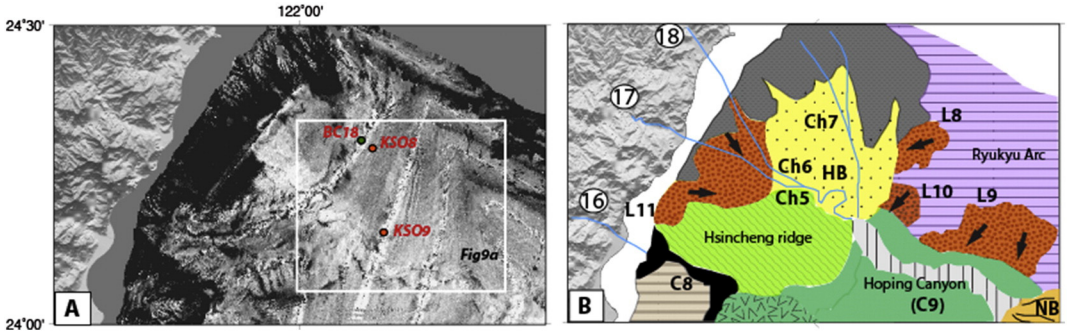

Fig. 8. A: Backscatter imagery of the northern sector. On backscatter images, dark tones indicate high backscatter; B: Mapping of the northern sector using backscatter imagery, seismic profiles and high resolution DEM. Annotated circles represent east coast rivers identified. 16. Liwu river, 17. Hoping river, 18. Nanao river, NB= Nanao Basin, HB= Hoping Basin. Key is the same as Fig. 3. See Fig. 2 for location of the northern sector.

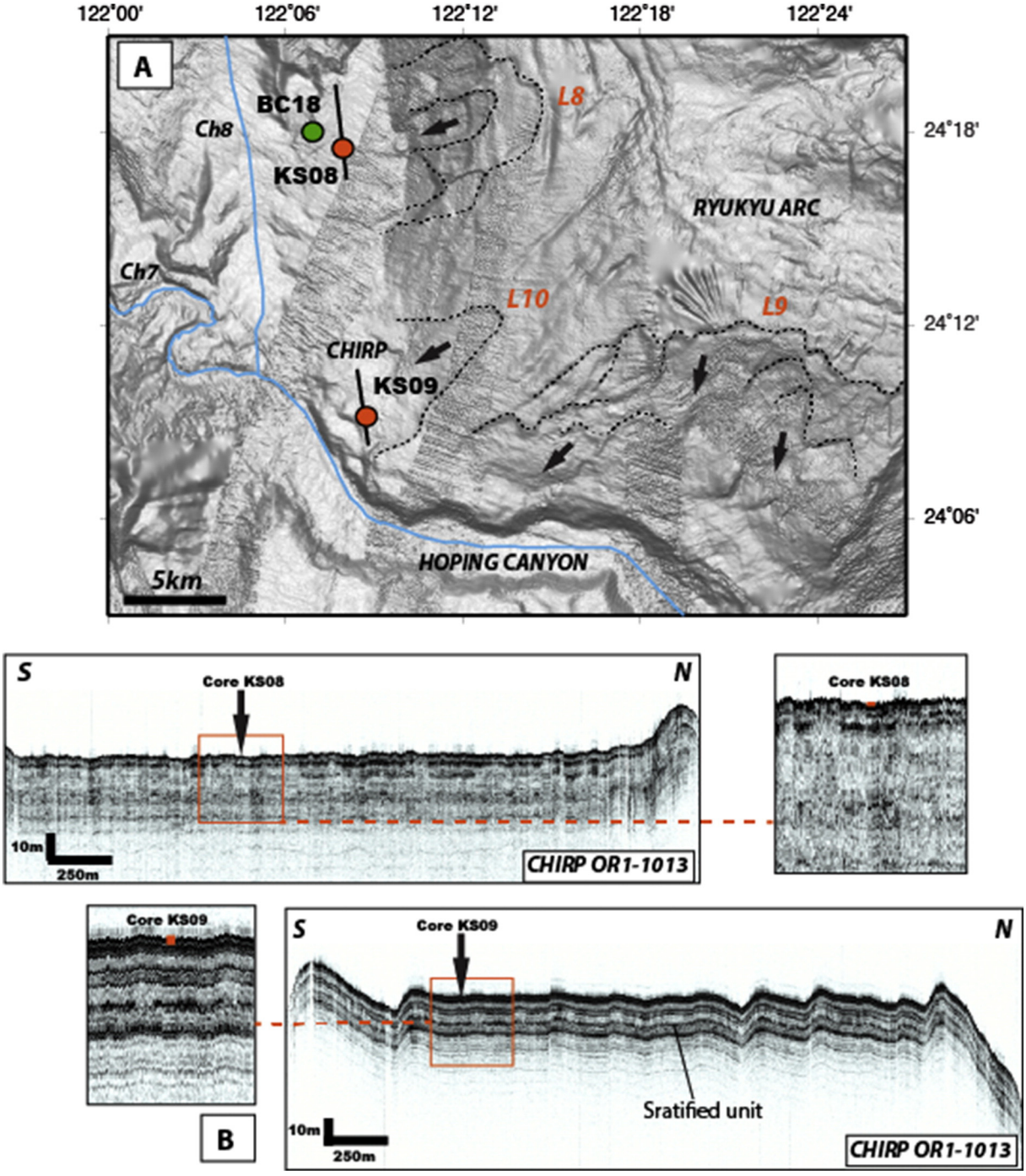

Fig. 9. A: High resolution DEM on the Ryukyu arc area showing landslides affecting the slope of the arc. Black arrows indicate the inferred landslides movements; B: CHIRP profiles displaying sedimentary levees. See Fig. 8 for location.

- *TIII*: thick to massive, fine sand to coarse sand lithogenic turbidites.

5.2.1. TI: Thin silty-clay lithogenic turbidites

It consists of 0.5–10 cm fining upward silty-clay sequences interbedded with Facies I. *TI* differs from Facies I (Hemipelagite) by being darker in color and coarser in grain size (from 15 to 25 μm instead of the 10 μm median grain size of hemipelagic sedimentation). The contact with hemipelagite is sharp and there is no evidence of basal erosion. The progressive grain-size evolution of the top of the silty-clay laminae indicates that they could correspond to thin and fine-grained turbidites. Chemical signature (shown by XRF) data, shows both slight positive anomalies in Fe and negative in Ca, on the coarser beds. The lithogenic fraction dominates the composition of the sand fraction (65%) (Fig. 12). The lithogenic fraction is composed by metamorphic rock fragments (40%), quartz grains (30%), slate (25%) and micas (5%) (Fig. 12). The other 35% of the coarser fraction are constituted by biogenic material with

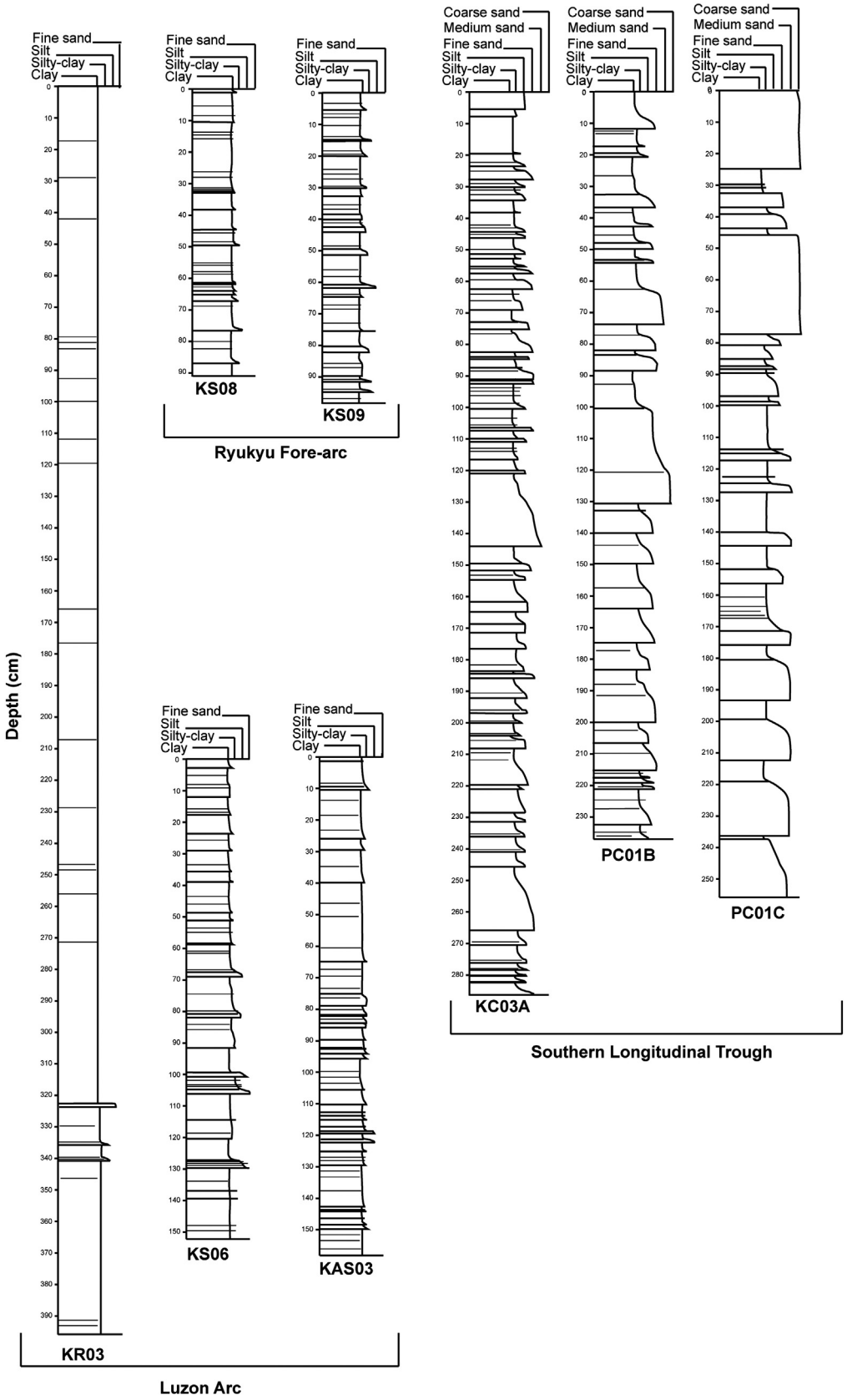

Fig. 10. Lithological description of cores. See Figs. 2, 3, 5 and 8 for locations of the coring sites.

benthic foraminifera (1%), vegetal remnants (5%), sponge spiculae (45%) and planktonic foraminifera (49%) (Fig. 12). Silty-clay turbidite may be interpreted as the subdivision T4 or T7 corresponding to low-density turbidity current defined by Stow and Shanmugam (1980). *TI* has been observed on cores KAS03, KS08 and KS09 (Figs. 10, 7 and 9 for cores location).

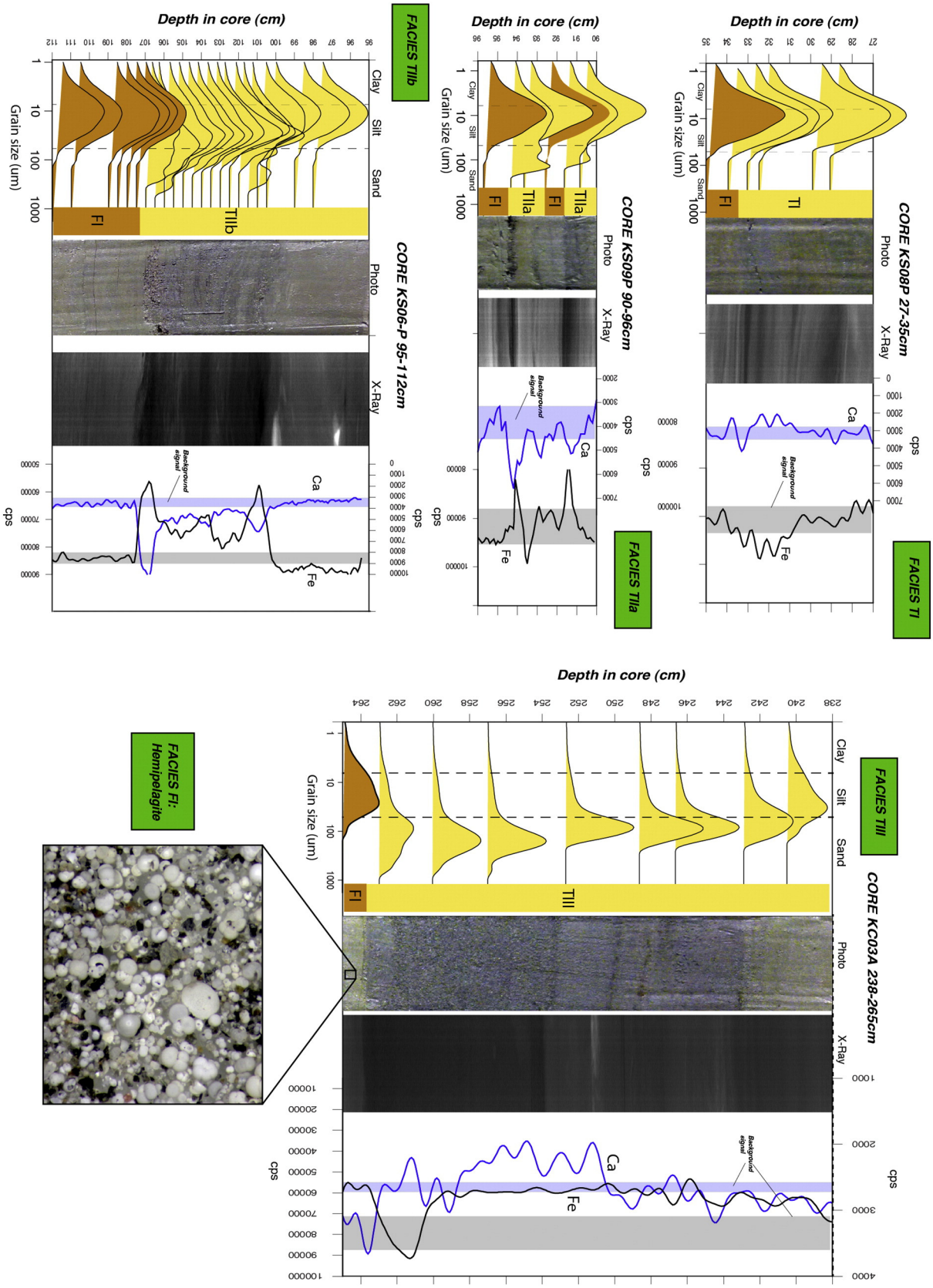

Fig. 11. Characterization of sedimentary facies using grain size distribution, X-rays and chemical analysis. The "background signal" of the XRF data represents the chemical signature of the hemipelagic sedimentation.

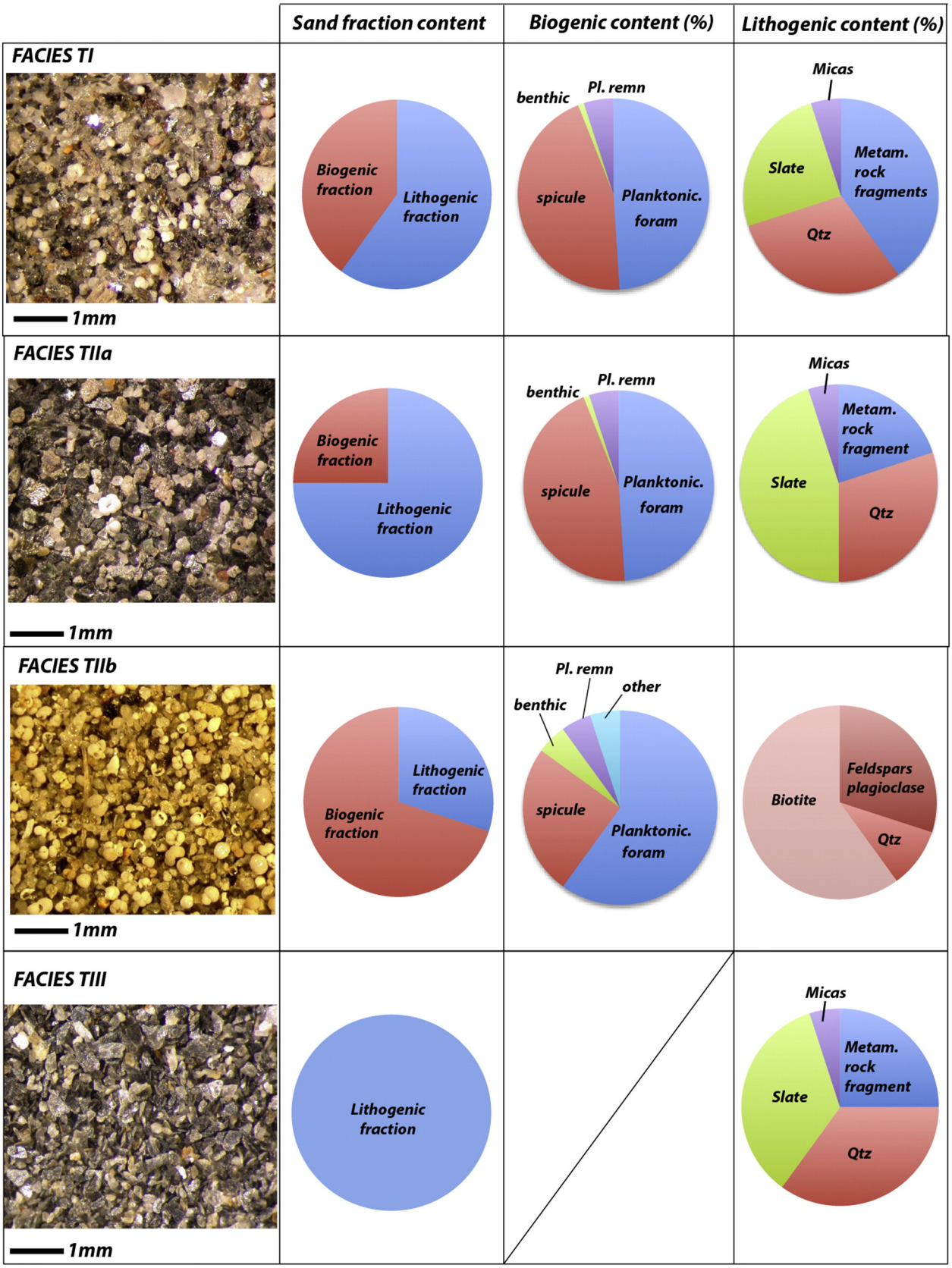

Fig. 12. Photography and relative composition (%) of the different turbidites facies identified corresponding to the coarser beds of turbidites sequences (fraction > 150 μm).

5.2.2. TII: Thin silty to fine sand turbidites

It is composed of 1 to 15 cm thick fining upward silty to fine sand sequences (Figs. 10, 11). The basal contact is usually sharp but in some cases there are evidences of erosional contact, characterized by a non-regular interface between turbidite base and hemipelagite facies (Fig. 11). *TII* is composed of a succession of silty to fine

sand turbidites alternating with thin hemipelagic intervals (Facies I) (Fig. 10).

5.2.2.1. TIIa: thin silty to fine sand lithogenic turbidites. Chemical analysis reveals positive Ca anomalies and negative Fe anomalies in coarser beds. The composition of the coarser fraction is mainly composed by lithogenic material (75%). The lithogenic fraction is composed by metamorphic rock fragments (20%), quartz (30%), slate (45%) and micas (5%). The other 25% of the coarser fraction are constituted by biogenic material with benthic foraminifera (1%), vegetal remnants (5%), sponge spiculae (45%) and planktonic foraminifera (49%) (Fig. 12). This turbidite facies may be assimilated to the subdivision Tb or Tc defined by Bouma (1962) and characteristic of low-density turbidity current. This facies is present in the cores KS09, KAS03 and KC03A (Figs. 10, 3, 7 and 9 for cores location), ORI-960-C5-G, ORI-969-3-P (Fig. 4A) as well as VM33-95 collected on the southern levee of the Taitung Canyon (Segment 3 on Fig. 3B).

5.2.2.2. TIIb: thin silty to fine sand biogenic turbidites. Chemical analysis reveals very clear positive Ca anomalies anticorrelated with negative Fe anomalies (relative to background signal, i.e Facies I) on coarser beds. In contrast with *TIIa*, the coarser fraction is composed by relatively high concentration of biogenic material (70%). This fraction contains mainly planktonic foraminifera (60%), sponge spicules (25%), benthic foraminifera (5%), plant remnants (5%) and other remnant organisms (5%). The lithogenic material is mainly constituted by feldspars plagioclase (60%), biotite (30%) and quartz (10%) (Fig. 12). This particular turbidite facies could also correspond to the subdivision Tb and Tc of the Bouma sequence (Bouma, 1962) that indicates a low-density turbidity flow. Facies *TIIb* has been observed only to core KS06 (Fig. 6 for core location).

5.2.3. TIII: thick to massive, fine sand to coarse sand lithogenic turbidites

TIII is characterized by a clear graded sand layer at the turbidite base, fining upward to silty sequences, usually >15 cm thick (Fig. 10). Chemical analysis show negative Ca and postivie Fe anomalies (relative to the hemipelagic signal) on coarser beds. The coarser fraction is only composed of lithogenic material (Fig. 12). We relate this turbidite facies to the subdivision Ta or Tb defined as medium-density turbidity current by Bouma (1962). Basal erosion is sometimes observed and characterized by an irregular surface between facies *TIII* and *TI*, suggesting erosion during the flow. This facies is characteristic of cores collected in the Southern Longitudinal Trough: KC03, P01B and P01C. The sedimentary cores described by Huang et al. (1992) (Fig. 3 for cores location) in the same area suggest that they are also characterized by facies *TIII* sometimes interbedded with very thin sequences of Facies I.

6. Discussion

6.1. Submarine gravity processes

The analysis of the morphology and seismic profiles along the eastern submarine slope of Taiwan shows a succession of erosional features (canyons, scarps) and depositional units related to submarine landslides and gravity flow processes. Three types of processes are distinguished: mass wasting of steep slope, channelized turbidity currents within canyons and channels, and unchannelized turbidity currents.

6.1.1. Mass wasting

On the continental slope of the Luzon Arc, several types of mass wasting were identified as slumps, slides and mass transport deposits (Figs. 4, 6, 8, 9). Slope failures vary from well-expressed scarp with short displacements (e.g, Figs. 4, 6) to superficial failures (e.g, Figs. 8, 9). The heads and walls of submarine canyons (e.g. Taitung canyon, L4 on segment 3, Figs. 3B and 4A) are also marked by slump scars suggesting a high contribution of small size submarine landslide in the incision of canyons. Slope failures are also observed at the base of the submarine slope, along turbidite systems as for example along channel-levees systems where sedimentation rates are high. The southern flank of the Chimei channel had collapsed displaying a well-defined scar (L7 on Figs. 5 and 7). There, the predisposing factor of gravity instability is related to both sediment overload with the levee aggradation and tectonic uplift.

6.1.2. Channelized turbidity currents

Location and morphology of canyon heads in connection with main river mouths indicate that the canyon initiation and evolution is clearly linked to the river sediment input, with a direct transfer from rivers to submarine canyons. Backscatter imagery and sedimentological data in the Southern Longitudinal Trough (SLT) show typical turbidite system with canyons, channel-levees system and lobe deposits. The high reflective gullied slopes of the SLT, the short shelf-break and the direct connection of major rivers with canyon heads show that this area is a by-pass region for channelized turbidity currents. The two sinuous channels Ch1 and Ch2, incised in the continuity of rivers 1 to 9 (Fig. 3B) are typical channel-levees systems (Fig. 3C and D). Turbidite deposits found in cores KC03A, PC01B and PC01C (Fig. 10) indicates that the volume and density of turbidity currents were variable, as shown by the relative grain size variation (from silty to coarse sand turbidites) and by the presence of erosive bases for some of the turbidites events. Likewise, the Hoping Basin (HB) shows similar features, interpreted as turbidite systems. The short shelf and the eroded gullied slope of the western slope of the HB indicate a by-pass zone. Downslope the Chimei Valley, a turbidite system develops including two sinuous channels (Ch3 and Ch4 Figs. 5, 7) and their associated sedimentary levees (Figs. 5 and 7). The presence of well-developed levees indicates the occurrence of large turbidity currents with a high content of fine-grained sediments (muddy) forming thick flows with high overflow capacity.

In turbidite systems, erosion and by-pass processes mainly occur inside canyons and channels axis as the same time as aggradation of overflow deposit with fine-grained sediments, building sedimentary levees on the sides of turbidite channel. In seismic lines, the Taitung and the Hoping channels are bordered by thick sediment accumulations with typical levee geometry, suggesting large overflow of turbidity currents feeding these sedimentary levees. Development of levees indicates mature sedimentary systems with recurrent turbidity currents and large volume of sediment provided to the canyon. This sedimentary architecture results from recurrent turbidity currents generated at the canyon heads. The development of mature turbidite systems is related to sediment source from rivers and a high contribution of climatic triggering mechanisms as hyperpycnal flows during typhoon events.

6.1.3. Unchannelized turbidity currents

The site KS06, located in a small confined basin without any connection to canyon or channel, present turbidite deposits indicating the triggering of local turbidity currents, resulting from small-size gravity instabilities (Figs. 5B, 6). Both seismic and sedimentological data show that this basin records turbidite deposits interbedded with hemipelagic sediments (Fig. 10). This basin is not connected to onland input and the slope may not play the role of sediment by-pass. Turbidity currents should be triggered on the slope itself. In this case, turbidity currents result from the transformation of small-size slump to debris flow and then to turbidity current. Sediment of the slope is transported and progressively suspended with the increase of the flow velocity. It is therefore an excellent site for paleoseismicity purposes (Lehu et al., 2015, submitted to Tectonophysics).

6.2. Tectonic control

6.2.1. Control on sedimentary paths

On tectonically active context, typical morphology is commonly observed in controlling the evolution of submarine canyons (Hampton et al., 1996; Laursen and Normark, 2002; McAdoo and Watts, 2004;

Mountjoy et al., 2009; Ratzov et al., 2012). The Taitung and Hualien canyon displays such features: a) V-shaped cross-sections, b) abrupt changes in direction (tributaries S1 and S2 of the Taitung canyon, Fig. 3B; tributaries S1 and S2 of the Hyalien canyon, Fig. 5B), and c) the pathway of Taitung canyon follows a reverse fault system before crossing the Luzon arc and associated thrust (Fig. 1B), and an active strike-slip fault in the oceanic basement (Schnurle et al., 1998; Sibuet et al., 2004) (Fig. 1B), whereas the Hualien canyon streams along the Ryukyu subduction front (Fig. 1B). Finally, numerous slope failures are observed on the walls of these canyons. All these features support that the path and morphology of the Taitung and Hualien canyons undergo a tectonic control. Contrastingly, the Hoping canyon displays different characteristics such as a U-shaped profile and exhibits a relative linear pathway. However, this canyon is located in the area where the deformation is paroxysmal suggesting that the Hoping canyon is also structurally controlled by faults cutting through the entire margin (Font and Lallemand, 2009).

6.2.2. Control on slope stability

Tectonic uplift and subsidence also play a great role on slope stability by progressively steepening the seafloor. Indeed, the slope stability represents an equilibrium between gravitational and resisting forces (Hampton et al., 1996). As the slope steepens, the shear stress (gravitational force) rises thus favoring instability. Additionnaly, intense tectonics may induce a fracturation and/or increase of pore water pressure (Gee et al., 2007), consequently weakening the seafloor, and reducing the shear strength and slope stability. Offshore eastern Taiwan, the submarine landslides are preferentially located on the steep slopes of the Luzon arc (17°) (e.g, L6; Fig. 6) and Ryukyu Arc (11°) (e.g, L8–L9; Fig. 9), both undergoing intense tectonic deformation. Such location is not random and supports the tectonic control on the location of landslides, by altering sediment slope stability and preconditioning the failures. Further investigation and data are however required to quantify the precise tectonic effects.

6.3. Seismic control

Numerous studies show that earthquakes have great impact on offshore sedimentation, by generating submarine landslides evolving into debris flows and turbidity currents. Such events were documented by the break of submarine cables shortly after earthquakes in various settings (Heezen and Ewing, 1955; Cattaneo et al., 2012), including the western Taiwan continental slope after the 2006 M-7 Pingtung earthquake (Hsu et al., 2008). Ground acceleration may either directly trigger relatively small but widespread failures and turbidity currents, play a longer term preconditioning factor for slope stability by strengthening or weakening the sediment cover (Ratzov et al., 2010). Seismicity offshore Taiwan is intense and frequent, but large slope failures such as L3 (Fig. 4), L6 (Fig. 6), L8, L9, L10 and L11 (Fig. 9) are relatively scarce; this observation supports that preconditioning by oversteepening but also probably earthquake repetition is required for large failures.

Contrastingly, numerous smaller-scale failures may result in the turbidite observed in the sedimentary cover. Based on core data collected in the Taiwan eastern margin, we established that in some specific location of the margin, earthquake shaking is their main triggering mechanism (Huh et al., 2004; Lehu et al., 2015, submitted to Tectonophysics). For example, site KS06 is located in an isolated intra-slope basin disconnected from any onland sediment input. The seismic facies shows a gentle surface with stratified reflectors that supports basin-infill revealed as fine-grained turbidites interbedded with hemipelagites (Figs. 10, 11) Moreover, the vicinity of KS06 site is characterized by the presence of several mass failures (Figs. 3, 4, 5, 6) that suggest slope instabilities due to tectonic and seismic shaking since this area is active and dissected by reverse faults (Malavieille et al., 2002). The dominance of biogenic content and the depletion in Fe (Figs. 10, 11) in turbidites confirm the lack of terrigenous input, and discards continental or shelf origin. The turbidites are therefore not related to hyperpycnal flows linked to major floods or typhoons. The most likely trigger is thus earthquake ground motion that is able to destabilize sediment at any water depths including deeper than the depth of storm waves effects. Following a similar rationale based on cores KS08 and KS09 (Fig. 2), seismic shaking appears as a dominant process for the sedimentation along the Ryukyu margin.

6.4. Typhoon control

Flood-induced turbidity currents result from hyperpycnal flow generation, when the density of the river charge is larger than the surrounding seawater (Mulder et al., 2003). In Taiwan, the rivers draining the orogen commonly discharge suspended sediment to the ocean at hyperpycnal concentration (Dadson et al., 2005) especially during typhoon-induced floods. In eastern Taiwan, the Taitung Canyon and the Hualien canyon are the only two canyons that have received important river sediment fluxes at hyperpycnal concentrations (Dadson et al., 2005). As previously described, the SLT is a proximal basin where major rivers deliver sediments during extreme floods and typhoon events (Fig. 3a). Moreover, the seafloor of the SLT is characterized by a well-developed turbiditic system suggesting a major climatic control. However, no data clearly indicate hyperpycnal flow deposits in the SLT. Indeed, when preserved, hyperpycnite are characterized by a coarsening upward from their base (Mulder et al., 2003), whereas turbidites described in core KC03A are not. Turbidite facies *TIII*, representative of most turbidites of the SLT, shows classical turbidite deposition (i.e fining-upward sequence) with sandy basal unit. Facies *TIII* is generally interbedded with very thin Facies I (Fig. 10) and shows that KC03A is characterized by stacked turbidites. Stacked turbidites suggest high events frequency that could correspond to floods that occur during the Asian monsoon season and typhoon activity that struck the east coast of Taiwan periodically. Alternatively, stacked turbidites may also correspond to individual events characterized by strong basal erosion that removes the underlying hemipelagite drape. According to the climatic context with intense flooding, the morphology with major rivers directly connected to the oceanic basin and especially with the 100% lithogenic Facies III that characterize core KC03A, we suggest that the SLT is mainly controlled by flood-induced turbidites.

7. Conclusion

In summary, the combined geophysical and sedimentological approaches used in this study have allowed us to observe that the offshore eastern Taiwan is characterized by a variety of sedimentary facies and erosional sedimentary processes from slided masses to turbidity currents. Turbidity current is the dominating sedimentary process in this active margin. Based on geophysical data, sedimentary levees and depositional basins cover about 60% of the study area and existing cores from these areas are dominated by cm to dm bedded sandy to silty turbidites and hemipelagites facies. In addition, according to the submarine morphological context, turbidity currents are generated by distinct controlling factors such as tectonic and climatic activity. Based on our sedimentary data and results, we define at least two end-members relative to turbidity currents initiation:

- Turbidity currents preconditioned by tectonic activity (oversteepening) and triggered by earthquakes shaking that initiate slope instabilities which likely deposit into isolated intra slope basin (e.g site KS06); and
- Turbidity currents likely driven by climatic activity such as extreme flood during typhoon, generated in close basin context directly connected with onland rivers (e.g site KC03A in the SLT).

This work, essentially base-mapped, thus represents a useful basis for future works such targeting coring of flow deposits on canyon/channel floor or identified landslides deposits, to recover material in

order to establish chronology of paleoearthquakes and paleoclimatic events.

Acknowledgments

We would like to thank Ching-Hui Tsai (NCU, Taiwan) Tei-Qei Lee (IES, Taiwan), Yinson Huang (IES, Taiwan), Shun-Wen Yu (NCU, Taiwan), Mo-Tsi Tsai (NCU, Taiwan), Don Su (NTU, Taiwan), Kuo-Yen Wei and his students (NTU, Taiwan), TORI workers, Stephane Dominguez (Montpellier Univ., France), Lucas Messales (UPMC, France), Slawek Giletycz (NCU, Taiwan), Irene Castro and many others who offered their help, advices, technical and expertise support. We are also grateful to the Captain and crew of the R/V Ocean Researcher I for their efficiency during the ORI-1013 and OR1-1048 surveys.

References

Biq, C., 1972. Dual-trench structure in the Taiwan–Luzon region. Proc. Geol. Soc. China 15, 65–75.
Bouma, A.H., 1962. Sedimentology of Some Flysch Deposits: A Graphic Approach to Facies Interpretation. vol. 168. Elsevier, Amsterdam.
Carter, L., Milliman, J., Talling, P., Gavey, R., Wynn, R., 2012. Near-synchronous and delayed initiation of long run-out submarine sediment flows from a record-breaking river flood, offshore Taiwan. Geophys. Res. Lett. 39 (12).
Cattaneo, A., Babonneau, N., Ratzov, G., Dan-Unterseh, G., Yelles, K., Bracene, R., De Lepinay, B.M., Boudiaf, A., Déverchere, J., 2012. Searching for the seafloor signature of the 21 may 2003 boumerdes earthquake offshore central Algeria. Nat. Hazards Earth Syst. Sci. 12 (7), 2159–2172.
Chen, K.-P., Tsai, Y.-B., 2008. A catalog of Taiwan earthquakes (1900–2006) with homogenized Mw magnitudes. Bull. Seismol. Soc. Am. 98 (1), 483–489.
Chen, C.-T.A., Liu, J.T., Tsuang, B.-J., 2004. Island-based catchment — the Taiwan example. Reg. Environ. Chang. 4 (1), 39–48.
Cheng, S.-N., Yeh, Y.-T., 1989. Catalog of the Earthquakes in Taiwan from 1604 to 1988. Bulletin IES, R-661. Institute of Earth Sciences, Taipei (255pp.).
Cheng, S.-N., Yeh, Y.-T., Yu, M.-S., 1996. The 1951 taitung earthquake in Taiwan. J. Geol. Soc. China Taiwan 39, 267–286.
Collot, J.-Y., Lewis, K., Lamarche, G., Lallemand, S., 2001. The giant Ruatoria debris avalanche on the northern Hikurangi margin, New Zealand: result of oblique seamount subduction. J. Geophys. Res. 106 (B9), 19271–19297.
Covault, J.A., Graham, S.A., 2010. Submarine fans at all sea-level stands: tectono-morphologic and climatic controls on terrigenous sediment delivery to the deep sea. Geology 38 (10), 939–942.
Dadson, S.J., Hovius, N., Chen, H., Dade, W.B., Lin, J.-C., Hsu, M.-L., Lin, C.-W., Horng, M.-J., Chen, T.-C., Milliman, J., Stark, C.P., 2004. Earthquake-triggered increase in sediment delivery from an active mountain belt. Geology 32 (8), 733.
Dadson, S., Hovius, N., Pegg, S., Dade, W.B., Horng, M.J., Chen, H., 2005. Hyperpycnal river flows from an active mountain belt. J. Geophys. Res. 110 (F4), F04016.
Einsele, G., 1996. Event deposits: the role of sediment supply and relative sea-level changes-an introduction. Sediment. Geol. 104 (1), 11–37.
Engdahl, E.R., Villaseñor, A., 2002. 41 global seismicity: 1900–1999. Int. Geophys. 81, 665–XVI.
Font, Y., Lallemand, S., 2009. Subducting oceanic high causes compressional faulting in southernmost Ryukyu forearc as revealed by hypocentral determinations of earthquakes and reflection/refraction seismic data. Tectonophysics 466 (3-4), 255–267.
Font, Y., Liu, C.-S., Schnurle, P., Lallemand, S., 2001. Constraints on backstop geometry of the southwest Ryukyu subduction based on reflection seismic data. Tectonophysics 333 (1-2), 135–158.
Galewsky, J., Stark, C.P., Dadson, S., Wu, C.-C., Sobel, a. H., Horng, M.-J., 2006. Tropical cyclone triggering of sediment discharge in Taiwan. J. Geophys. Res. 111 (F3), F03014.
Ge, X., Li, T., Zhang, S., Peng, M., 2010. What causes the extremely heavy rainfall in Taiwan during typhoon morakot (2009)? Atmos. Sci. Lett. 11 (1), 46–50.
Gee, M., Uy, H., Warren, J., Morley, C., Lambiase, J., 2007. The Brunei slide: a giant submarine landslide on the north west Borneo margin revealed by 3D seismic data. Mar. Geol. 246 (1), 9–23.
Hampton, M., Lee, H.J., Locat, J., 1996. Submarine landslides. Rev. Geophys. 34 (1), 33–59.
Heezen, B.C., Ewing, M., 1955. Orleansville earthquake and turbidity currents. AAPG Bull. 39 (12), 2505–2514.
Hetland, E.A., Wu, F.T., 2001. Crustal structure at the intersection of the Ryukyu trench with the arc-continent collision in Taiwan: results from an offshore-onshore seismic experiment. Terr. Atmos. Ocean. Sci. 12 (SUPP), 231–248.
Hsin, Y.-C., Wu, C.-R., Shaw, P.-T., 2008. Spatial and temporal variations of the Kuroshio east of Taiwan, 1982–2005: a numerical study. J. Geophys. Res. Oceans 113 (C4).
Hsu, S.-K., Kuo, J., Lo, C.-L., Tsai, C.-H., Doo, W.-B., Ku, C.-Y., Sibuet, J.-C., 2008. Turbidity currents, submarine landslides and 2006 Pingtung earthquake off SW Taiwan. Terr. Atmos. Ocean. Sci. 19, 767–772.
Huang, C., Shyu, C., Lin, S., Lee, T., Sheu, D., 1992. Marine geology in the arc-continent collision zone off southeastern Taiwan: implications for late Neogene evolution of the coastal range. Mar. Geol. 107, 183–212.
Huh, C.-A., Su, C.-C., Liang, W.-T., Ling, C.-Y., 2004. Linkages between turbidites in the southern Okinawa trough and submarine earthquakes. Geophys. Res. Lett. 31, 2–5.
Huh, C.-A., Su, C.-C., Wang, C.-H., Lee, S.-Y., Lin, I.-T., 2006. Sedimentation in the southern Okinawa trough-rates, turbidites and a sediment budget. Mar. Geol. 231 (1), 129–139.
Kao, S., Milliman, J., 2008. Water and sediment discharge from small mountainous rivers, Taiwan: the roles of lithology, episodic events, and human activities. J. Geol. 116 (5), 431–448.
Lallemand, S.E., Tsien, H.-H., 1997. An introduction to active collision in Taiwan. Tectonophysics 274, 1–4.
Lallemand, S.E., Liu, C.-S., Font, Y., 1997. A tear fault boundary between the Taiwan orogen and the Ryukyu subduction zone. Tectonophysics 274 (1), 171–190.
Lallemand, S., Liu, C.-S., Schntirle, P., Malavieille, J., Crew, A.S., c., 1999. Partition caused by oblique convergence. Tectonics 18 (2), 231–247.
Lallemand, S., Theunissen, T., Schnürle, P., Lee, C.-S., Liu, C.-S., Font, Y., 2013. Tectonophysics indentation of the Philippine Sea plate by the Eurasia plate in Taiwan: details from recent marine seismological experiments. Tectonophysics 594, 60–79.
Laursen, J., Normark, W.R., 2002. Late quaternary evolution of the San Antonio submarine canyon in the central Chile forearc (33 s). Mar. Geol. 188 (3), 365–390.
Lehu, R., Lallemand, S., Hsu, S.-K., Lin, A.T., Ratzov, G., Babonneau, N., Dezileau, L., 2015. Reconstructing 2,700 years earthquakes history using deep-sea turbidites offshore eastern Taiwan. Tectonophysics (in revisions).
Li, Y.-H., 1976. Denudation of Taiwan island since the Pliocene epoch. Geology 4 (2), 105–107.
Lin, Y.-L., Ensley, D.B., Chiao, S., Huang, C.-Y., 2002. Orographic influences on rainfall and track deflection associated with the passage of a tropical cyclone. Mon. Weather Rev. 130 (12).
Liu, J., Liu, C., Xu, K., Milliman, J., Chiu, J., Kao, S., Lin, S., 2008. Flux and fate of small mountainous rivers derived sediments into the Taiwan Strait. Mar. Geol. 256 (1-4), 65–76 (Dec.).
Locat, J., Lee, H.J., 2002. Submarine landslides: advances and challenges. Can. Geotech. J. 39 (1), 193–212.
Malavieille, J., Lallemand, S., Dominguez, S., Deschamps, A., Lu, C., Liu, C., Schnürle, P., Hsu, J., Liu, S., Sibuet, J., et al., 2002. Arc-continent collision in Taiwan new marine observations and tectonic evolution. Geol. Soc. Am. Spec. Pap. 189–213.
Masson, D.G., Harbitz, C.B., Wynn, R.B., Pedersen, G., Lø vholt, F., 2006. Submarine landslides: processes, triggers and hazard prediction. Philos. Transact. A Math. Phys. Eng. Sci. 364 (1845), 2009–2039.
McAdoo, B., Watts, P., 2004. Tsunami hazard from submarine landslides on the oregon continental slope. Mar. Geol. 203 (3), 235–245.
Mcintosh, K.D., Nakamura, Y., 1998. Crustal structure beneath the nanao forearc basin from taicrust mcs/obs line 14. Terr. Atmos. Ocean. Sci. 9 (3), 345–362.
McIntosh, K., Nakamura, Y., Wang, T.-K., Shih, R.-C., Chen, A., Liu, C.-S., 2005. Crustal-scale seismic profiles across Taiwan and the western Philippine Sea. Tectonophysics 401 (1), 23–54.
Milliman, J.D., Syvitski, J.P., 1992. Geomorphic/tectonic control of sediment discharge to the ocean: the importance of small mountainous rivers. J. Geol. 525–544.
Mountjoy, J.J., Barnes, P.M., Pettinga, J.R., 2009. Morphostructure and evolution of submarine canyons across an active margin: Cook Strait sector of the Hikurangi Margin, New Zealand. Mar. Geol. 1–24.
Mulder, T., Alexander, J., 2001. The physical character of subaqueous sedimentary density flows and their deposits. Sedimentology 48 (2), 269–299.
Mulder, T., Cochonat, P., 1996. Classification of offshore mass movements. J. Sediment. Res. 66 (1), 43–57.
Mulder, T., Syvitski, J.P., Migeon, S., Faugeres, J.-C., Savoye, B., 2003. Marine hyperpycnal flows: initiation, behavior and related deposits. A review. Mar. Pet. Geol. 20 (6), 861–882.
Piper, D.J., Normark, W.R., 2009. Processes that initiate turbidity currents and their influence on turbidites: a marine geology perspective. J. Sediment. Res. 79 (6), 347–362.
Ramsey, L., Hovius, N., Lague, D., Liu, C.-S., 2006. Topographic characteristics of the submarine Taiwan orogen. J. Geophys. Res. 111 (F2), 1–21.
Ratzov, G., Collot, J.-Y., Sosson, M., Migeon, S., 2010. Mass-transport deposits in the northern Ecuador subduction trench: result of frontal erosion over multiple seismic cycles. Earth Planet. Sci. Lett. 296 (1), 89–102.
Ratzov, G., Sosson, M., Collot, J.-Y., Migeon, S., 2012. Late quaternary geomorphologic evolution of submarine canyons as a marker of active deformation on convergent margins: the example of the south colombian margin. Mar. Geol. 315, 77–97.
Romans, B.W., Normark, W.R., McGann, M.M., Covault, J.A., Graham, S.A., 2009. Coarse-grained sediment delivery and distribution in the holocene santa monica basin, california: implications for evaluating source-to-sink flux at millennial time scales. Geol. Soc. Am. Bull. 121 (9-10), 1394–1408.
Schnurle, P., Liu, C.-S., Lallemand, S., Reed, D., 1998. Structural controls of the taitung canyon in the huatung basin east of Taiwan. Terr. Atmos. Ocean. Sci. 9, 453–473.
Schnürle, P., Liu, C.-S., Lallemand, S.E., Reed, D.L., 1998. Structural insight into the south Ryukyu margin: effects of the subducting gagua ridge. Tectonophysics 288 (1), 237–250.
Seno, T., Stein, S., Gripp, A.E., 1993. A model for the motion of the Philippine sea plate consistent with nuvel-1 and geological data. J. Geophys. Res. Solid Earth 98 (B10), 17941–17948.
Sibuet, J.-C., Hsu, S.-K., Normand, A., 2004. Tectonic significance of the Taitung Canyon, Huatung Basin, east of Taiwan. Mar. Geophys. Res 25 (1–2), 95–107 (Springer).
Stow, D.A., Shanmugam, G., 1980. Sequence of structures in fine-grained turbidites: comparison of recent deep-sea and ancient flysch sediments. Sediment. Geol. 25 (1), 23–42.
Suppe, J., 1984. Kinematics of arc-continent collision, flipping of subduction, and back-arc spreading near Taiwan. Mem. Geol. Soc. China 6, 21–33.
Theunissen, T., Font, Y., Lallemand, S., Liang, W.-T., 2010. The largest instrumentally recorded earthquake in Taiwan: revised location and magnitude, and tectonic significance of the 1920 event. Geophys. J. Int. 183 (3), 1119–1133.

Tsou, C.-Y., Feng, Z.-Y., Chigira, M., 2011. Catastrophic landslide induced by typhoon morakot, shiaolin, Taiwan. Geomorphology 127 (3), 166–178.
Wang, T.K., Chiang, C.-H., 1998. Imaging of arc–arc collision in the Ryukyu forearc region offshore hualien from taicrust obs line 16. Terr. Atmos. Ocean. Sci. 9 (3), 329–344.
Wang, T.K., Lin, S.-F., Liu, C.-S., Wang, C.-S., 2004. Crustal structure of the southernmost Ryukyu subduction zone: OBS, MCS and gravity modelling. Geophys. J. Int. 157 (1), 147–163.
Wu, C.-C., Kuo, Y.-H., et al., 1999. Typhoons affecting Taiwan: current understanding and future challenges. Bull. Am. Meteorol. Soc. 80 (1), 67–80.
Wu, Y.-M., Chang, C.-H., Zhao, L., Teng, T.-L., Nakamura, M., 2008. A comprehensive relocation of earthquakes in Taiwan from 1991 to 2005. Bull. Seismol. Soc. Am. 98 (3), 1471–1481.
Wu, C.-H., Chen, S.-C., Chou, H.-T., 2011. Geomorphologic characteristics of catastrophic landslides during typhoon morakot in the Kaoping watershed, Taiwan. Eng. Geol. 123 (1-2), 13–21.